

Flow Path Optimization for a Typical 20 Cells Solid Oxide Fuel Cell Stack with Co- and Counter- Flow Arrangement Patterns

D.F. Chen¹, Z.Y. Chen¹, J. Li¹, J.Q. Zhang¹, K. Liu^{2,*}

¹ School of Power and Energy, Jiangsu University of Science and Technology, Zhenjiang 212003, China

² School of Naval Architecture and Ocean Engineering, Jiangsu University of Science and Technology, Zhenjiang 212003, China

*E-mail: dfchen01@163.com, kunliu@just.edu.cn

Received: 22 November 2018 / Accepted: 5 January 2019 / Published: 7 February 2019

This paper focuses on air and fuel flow path optimizations for a specific 20 cells modular stack operated in both co- and counter-flow arrangement patterns. Stack uniformity index is used to characterize air (or fuel) flow distribution quality among the piled 20 cell units. Standard deviation factor for the mass flow rates obtained by rib channels is adopted to present the flow distribution quality over each cell surface. Then, the effect of the geometric parameters, such as air and fuel manifold configurations, manifold radii, feed and exhaust header widths, on the flow distribution qualities within the specific stack design are studied to achieve the optimized choice for both co- and counter-flow arrangement patterns. Predicted result shows that the best counter-flow arrangement pattern for the 20 cells stack is that 2in3out manifold configurations for both air and fuel flow paths. The best co-flow arrangement pattern for the 20 cells stack is that 2in3out manifold configuration for air flow path and 3in2out manifold configuration for fuel flow path. Proper fuel/air flow manifold radii and feed/exhaust header widths for different flow distribution qualities within the specific 20-cell stack are also provided.

Keywords: SOFC modular stack; calculated fluid dynamics; counter- and co-flows; rib channels.

1. INTRODUCTION

Planar solid oxide fuel cell (SOFC) is considered to be one of the promising power conversion devices due to the advantages of fuel flexibility [1], compactness [2-4], high volumetric and gravimetric power densities [5-7], and so on. Fig. 1 shows a typical planar SOFC stack design [8], in which several unit cells are connected in series. The structure of this planar SOFC stack is composed of three important parts: i) membrane electrode assembly (MEA), which includes porous cathode,

dense electrolyte and porous anode [9-11]. This is the core part of the SOFC to convert the chemical energy of reactants into electric energy directly [12-14]; ii) the interconnect plate. It consists of many parallel channels dug in both upside and downside. Thus, it can be divided into three components: interconnect, solid ribs and rib channels. A proper interconnect plate in a SOFC stack should satisfy two major functions: a) collect and conduct the produced current within each MEA; b) separate the fuel and oxidant flows and respectively distribute them over the MEA; iii) inlet and outlet manifolds. Taking the stack design in Fig. 1 as an example, five manifolds are aligned in both sides of the interconnect plate, respectively. Thus, this stack structure can support both the counter- and co-flow arrangement designs.

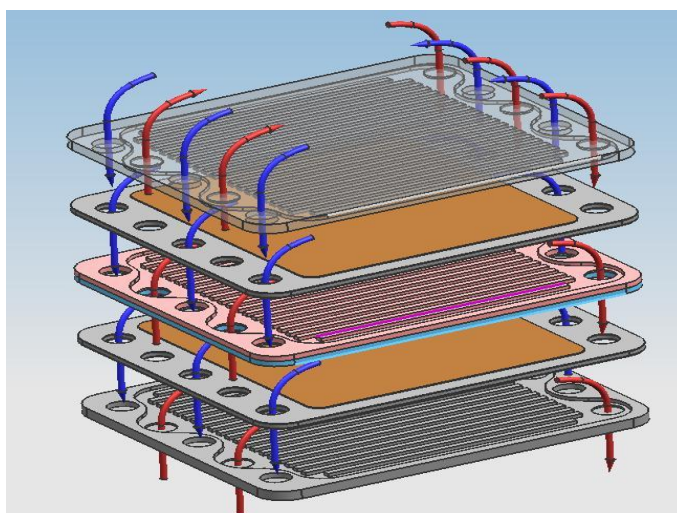


Figure 1. Illustration of a typical planar SOFC stack design, which can be operated in both co- and counter-flow arrangement patterns.

One challenge in developing the planar SOFC technology is to achieve and maintain a high performance during the entire stack lifetime. In the past decade, a large number of SOFC stack configurations have been proposed [15-17] and analyzed through analytical [18, 19], numerical [20-22] and experimental [23-27] approaches. The flow transport mechanics within the SOFC stack were well studied, and many valuable guidelines for the stack structure design were obtained. Boersma and Sammes [28] proposed a primitive analytical model to predict the flow distribution conditions along the height of a fuel cell stack. The gas-phase fluid transport was represented using a number of hydraulic resistances that were linked in series or parallel. Ko had optimized the fuel flow rate to improve the stability of the Ni-based SOFC [29]. The assembly process was well simulated by a 3D large scale model to obtain the distribution of stress and deformation of fuel cell stack components [30]. Recknagle had compared the flow and temperature distributing characteristics of the cross-flow, counter-flow and co-flow stack designs, respectively [31]. Although the stack with cross-flow configuration had many outstanding advantages, it might suffer from the highest temperature gradient. There exists “hot island” located at the corner between the fuel inlet and air outlet, and the minimum of fuel concentration would be founded at its diagonal side. For both the counter- and co-flow configurations, the temperatures would increase along their air flowing directions [32].

In the past decades, most of the efforts were focused on optimizing many specific SOFC stacks, in which dozens of fuel cell units were piled in a large scale stack to achieve high voltage and power outputs [33]. It is necessary to mention that these types of large scale stacks would suffer from some disadvantage in repairing and maintaining stable power output, especially while any cell unit or component within the large scale stack fails. A modular short SOFC stack with 0.5~1.5 kW power output may have a great potential to commercialize the SOFC stacks [34]. Obviously, once modular short SOFC stack can be standardized with a proper cell number (or output power), many auxiliary systems, such as heat and electric managements and fuel/air supply systems, would be designed and optimized independently in the near future. Furthermore, the performance comparisons among different planar SOFC stack designs will become convenient because of the similar stack scale requirement.

In this work, three-dimensional computational fluid dynamics (CFD) simulation for the fuel/air flow paths within a 20 cells modular SOFC stack is developed to optimize both the fuel and air flow distribution paths for both counter- and co-flow arrangement patterns. The optimization process considers the uniformities of flow distributions in two scale levels, among piled cell units and over each unit cell surfaces, respectively. Several geometric parameters, such as the air/fuel flow manifold configurations, manifold sizes, feed/exhaust header sizes, etc. are investigated. The optimized results would be useful for providing generality in practical application of developing modular planar SOFC stacks that are operated in co- or counter-flow arrangement.

2. THEORY AND SIMULATION

2.1. 3D Flow paths within the modular SOFC stacks

This paper focus on a typical 20 cells modular SOFC stack with 100 mm×107.5 mm MEA area, and five manifold holes in each side of the interconnect plate. As shown in Fig. 1, red arrows indicate fuel-flow directions.

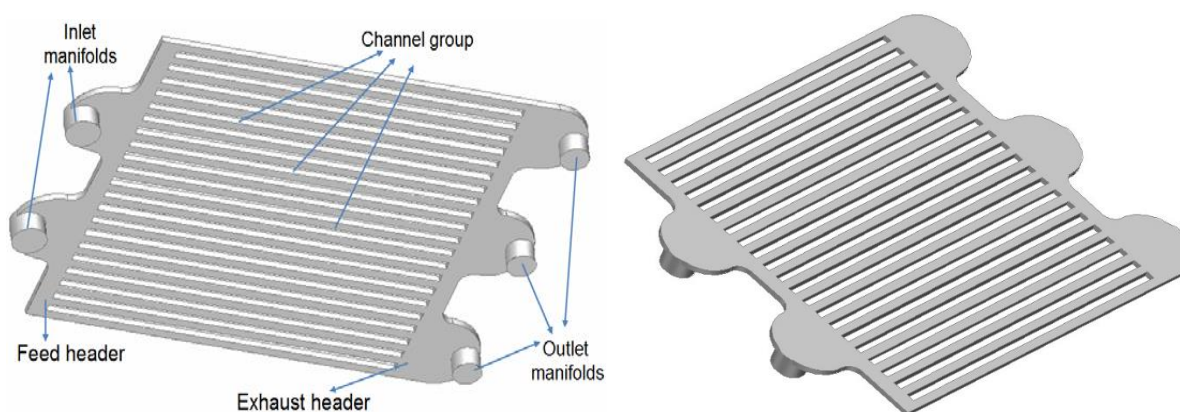


Figure 2. Diagrammatic sketch for air (or fuel) rib channels over each SOFC unit surfaces from different angle views.

The configuration of fuel flow manifolds distribution is labeled as ‘2in3out’. It means two inlet manifolds in one side and three outlet manifolds in the opposite side. Similarly, there are blue arrows for the air-flow directions, and the configuration of air flow manifold distribution is called as ‘2in3out’ too. Fig. 2 shows the flow path of rib channels over each SOFC unit surface in different angle views; and the relevant geometric parameters are indicated in table 1.

As illustrated in Fig. 2, both the inlet/outlet manifolds and rib channels contribute to the whole flow distributing path. The internal flow distributing process within the flow path can be assessed through two levels. i) the flow distributing quality among the piled cell units. Two parallel inlet manifolds lead the air/fuel into each cell unit; and then transport the excess flow to the next cell unit. ii) the flow distributing quality among the rib channels. Flow paths over each cell unit consist of the feed header, 22 rectangular flow channels divided by 21 solid ribs, and the exhaust header. When the flow is induced into each cell unit, it is collected at feeding header firstly. Then it is further distributed into the rib channels over the SOFC surface. Finally, the consumed air (or fuel) flow is collected in exhaust header and pushed out to the outlet manifolds.

Table 1. Geometric parameters of a typical planar fuel cell stack corresponding to figure 1.

Components	Fuel side	Air side
MEA area	100 mm×107.5 mm	100 mm×107.5 mm
Height of the cell layer	6.0 mm	6.0 mm
Inlet/outlet manifolds (radius×height)	$r_{in} \times 4.5$ mm	$r_{in} \times 4.5$ mm
Feed header (width×height)	5 mm×107.5 mm	5 mm×107.5 mm
Solid Rib (width×height)	2.5 mm×1.5 mm	2.5 mm×1.5 mm
Rib Channel (width×height)	2.5 mm×1.5 mm	2.5 mm×1.5 mm
Exhaust header (width×height)	5 mm×107.5 mm	5 mm×107.5 mm

As illustrated in Fig. 3, this modular short stack structure can support four types of flow arrangement patterns, and the relevant labels are collected in table 2. Taking Type 3 for example, the flow arrangement pattern is co-flow with 2in3out for the air flow manifolds and 3in2out for the fuel flow manifolds. Here, 2in3out means there are 2 inlet manifolds and 3 outlet manifolds located at the opposite sides of the interconnect plate.

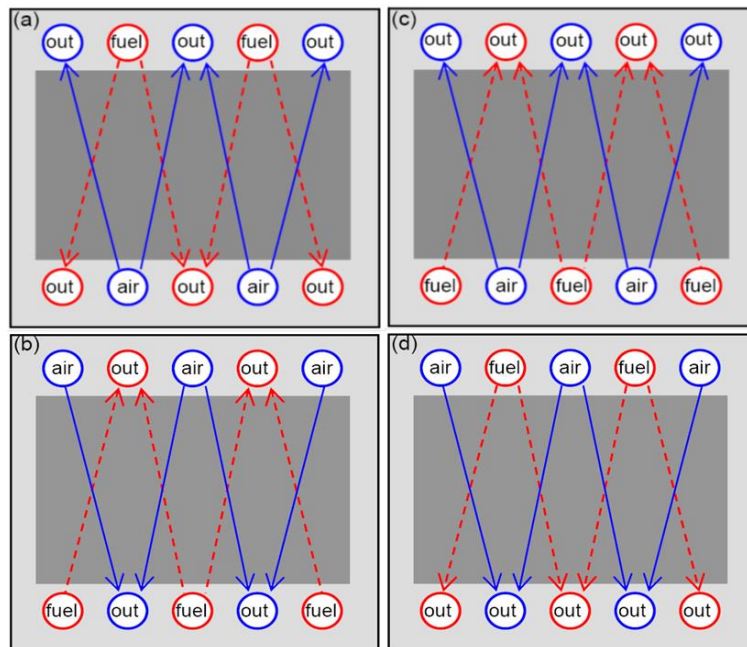


Figure 3. Four types of flow arrangement patterns corresponding to the stack structure of figure 1.

Table 2. Types of flow arrangement patterns for the planar SOFC stack design in figure 1.

Type	Flow arrangement	Configuration of air flow manifolds	Configuration of fuel flow manifolds
1	Counter-flow	2in3out	2in3out
2	Counter-flow	3in2out	3in2out
3	Co-flow	2in3out	3in2out
4	Co-flow	3in2out	2in3out

The 3D fluid dynamics models for the 20 cells modular short planar SOFC stacks with different flow arrangement patterns are developed and calculated based on the mass continuity and momentum conservation equations,

$$\frac{\partial \rho}{\partial t} + \nabla \cdot (\rho \mathbf{u}) = 0, \tag{1}$$

$$\frac{\partial \rho \mathbf{u}}{\partial t} + \nabla \cdot (\rho \mathbf{u} \otimes \mathbf{u}) = -\nabla p + \nabla \cdot \tau, \tag{2}$$

where \mathbf{u} is flow velocity. p is local static pressure. τ is stress tensor. ρ is flow density. The gas flow within the stack is assumed to be ideal gas, and Sutherland's law is used to evaluate the kinetic viscosity of the air (or fuel) flow as,

$$\mu_\alpha \approx \mu_\alpha^0 \left(\frac{T}{T_0} \right)^{1.5} \frac{T_0 + \delta_\alpha}{T + \delta_\alpha}, \tag{3}$$

where δ_α is the Sutherland's constant of species α which can be derived from reported experiment datum ($\delta_{\text{air}} = 111, \delta_{\text{H}_2} = 97, \delta_{\text{H}_2\text{O}} = 1064$ at $T_0 = 273$ K) [35]. μ_α^0 is pre-factor. Then, the viscosity of

air and fuel flows at 1073 K can be calculated to be 4.16×10^{-5} and 2.1×10^{-5} kg m⁻¹ s⁻¹, respectively.

Three different boundary conditions are adopted during the calculating: i) the net total mass flow rate at the inlet manifold entrances $\dot{m}_{\text{mix_in}}$ is fixed. Then, the inlet velocity the entrances can be specified as $u_{\text{in}} = \dot{m}_{\text{mix_in}} / (\rho A_{\text{in}})$. A_{in} is the total cross section areas of all inlet manifold entrances; ii) a reference pressure at the outlet manifold exit is addressed; iii) the no-slip boundary conditions are used to the flow-wall boundaries.

For a SOFC stack with power output around 1 kW, the total air and fuel feeding rate are approximately $\dot{m}_{\text{air_in}} = 327$ SLPM (standard liter per minute) and $\dot{m}_{\text{fuel_in}} = 60.7$ SLPM, respectively.

$$\dot{m}_{\text{air_in}} = \frac{N_l i_{\text{op}} A M_{\text{air}}}{4F \eta_{\text{O}_2} x_{\text{O}_2}}, \quad \dot{m}_{\text{fuel_in}} = \frac{N_l i_{\text{op}} A M_{\text{fuel}}}{2F \eta_{\text{H}_2} x_{\text{H}_2}}, \quad (4)$$

where $x_{\text{O}_2} = 21\%$ is the mole fraction of oxygen in air. $x_{\text{H}_2} = 97\%$ is the mole fraction of hydrogen in hydrogen-steam fuel mixture. $N_l = 20$ is the number of unit cells in a modular stack. F is Faraday constant. M_{air} and M_{fuel} are the molecular weights of air and fuel mixture, respectively. The average current density through MEA is about $i_{\text{op}} = 7000$ A m⁻² with the oxygen utilization of $\eta_{\text{O}_2} = 30\%$ and fuel utilization of $\eta_{\text{H}_2} = 70\%$

Commercial software FLUENT is used for simulating the flow distributing characteristics within the 20 cells modular SOFC stack. Reynolds numbers ($Re = \rho u D / \mu$) within the inlet manifolds are estimated to determine the flow type (i.e., laminar flow model for $Re < 2000$ and turbulent flow model for $Re \geq 2000$). The convergence target is set as 10^{-6} .

2.2. Important parameters for the flow optimization

Generally, the following three factors are considered to be very important for a planar SOFC to achieve high performance and long overall stack lifetime,

i) **Minimum flow rate among unit cells Γ** : as a typical planar stack consists of several piled cell units (shown in Fig. 1), each unit cell should produces similar total electric current. The unit cell that gets the least reactant flow rate should play the major role in determining the overall stack performance. Thus, the minimum reactant flow rate among the piled cell layers is a key factor to represent gas flow distribution quality among the piled cell layers. It is defined as the stack flow uniformity index,

$$\Gamma = \min(\dot{m}_{l,1} : \dot{m}_{l,N_l}), \quad (5)$$

Denoting the mass-flow rate obtained by i -th unit cell unit as $\dot{m}_{l,i}$ ($1 \leq i \leq N_l$). The normalized form can be got as $\dot{m}_{l,i}^* = \dot{m}_{l,i} / \bar{\dot{m}}_l$. $\bar{\dot{m}}_l$ is the mean flow rate among the piled cells (i.e., $\dot{m}_{\text{air_in}} / N_l$ at the air side, $\dot{m}_{\text{fuel_in}} / N_l$ at the fuel side). Generally, using normalized item to present the flow distributing quality can provide convenience in comparing the performances among the planar SOFC stack with different designs, scales or operation parameters.

ii) **Pressure drop Δp** : the pressure deviation between inlet manifold entrance and outlet manifold exit is also an important factor to evaluate the quality of stack design. Because high net pressure drop throughout the stack means that additional power would be consumed for driving

compressors [19].

iii) **Standard deviation of the rib channel flow rates** σ_c : the distribution quality of air/fuel flow among rib channels is another important factor to determine SOFC stack performance. As displayed in Fig. 2, the flow distributing channels over each cell layer surface are no longer connected in series. As they are connected in parallel, the rib channel that received the minimum air/fuel flow rate should not exclusively determine the cell unit performance. In contrary, minimal flow rate distributing variation among the rib channels is the key factor to ensure the uniformly distribution of current-induced degradation over the cell unit surface. This is important to reduce the temperature gradient over the SOFC unit surface [36]. Thus, the standard deviation factor of mass flow rates among the rib channels is defined to represent the flow distributing quality on single cell unit [23],

$$\sigma_c = \left\{ \frac{1}{N_c} \sum_{j=1}^{N_c} (n_{c,j}^{\&}-1)^2 \right\}^{1/2}, \quad (6)$$

where $N_c = 22$ is rib channel number within each repeat cell layer. Normalized item $n_{c,j}^{\&}$ can be calculated by $n_{c,j}^{\&} = n_{c,j}^{\&} / \text{ave}(n_{c,1}^{\&} : n_{c,N_c}^{\&})$, in which $n_{c,j}^{\&}$ is the mass flow rate obtained by the j -th rib channel within each cell unit.

3. RESULT AND DISCUSSION

Table 3. Case indexes for the air/fuel flow path models with different geometric parameters.

Air flow paths			
Case index	Configuration	r_{in} (mm)	Header width (mm)
case 1-5	2in3out & $r_{out}=r_{in}$	4, 5, 6, 7, 8	5
case 6-10	3in2out & $r_{out}=r_{in}$	4, 5, 6, 7, 8	5
case 11-14	3in2out & $r_{out}=1.2r_{in}$	4, 5, 6, 7	5
case 15-17	2in3out & $r_{out}=r_{in}$	6	2.5, 10, 15
Fuel flow paths			
Case index	Configuration	r_{in} (mm)	Header width (mm)
case 21-25	2in3out & $r_{out}=r_{in}$	4, 5, 6, 7, 8	5
case 26-30	3in2out & $r_{out}=r_{in}$	4, 5, 6, 7, 8	5
case 31-34	3in2out & $r_{out}=1.2r_{in}$	4, 5, 6, 7	5
case 35-37	2in3out & $r_{out}=r_{in}$	6	2.5, 10, 15
case 38-40	3in2out & $r_{out}=1.2r_{in}$	6	2.5, 10, 15

The 20 cells modular short SOFC stack is designed to produce a power around 1 kW. 3D

numerical models for the air and fuel flow paths are separately developed to investigate the effects of several geometric factors (i.e., manifold configurations, inlet/outlet manifold radii, and feed/exhaust header sizes) on the flow distributing qualities within the stack by both stack uniformity index on stack level and standard deviation factor on cell unit level. Table 3 lists the relevant case indexes for the air and fuel flow path models with different geometric parameters.

Taking the 3D air flow path model with 2in3out manifold configuration, $r_{out}=r_{in}=4$ mm (i.e., case 1) and $\dot{m}_{air_in}=327$ SLPM as an example. Fig. 4a shows the corresponding 3D flow field model of air flow path within the 20 cells stack. Then, around 1.6 million hexahedral meshes are addressed to the 3D model to figure out the detail flow characteristics within the flow path accurately.

In Fig. 4b, the relevant static pressure p distribuion within the air flow path refferencing to the 0 pressure at the outlet manifold exit is figured out. As shown in the figure, p within both inlet and outlet manifolds increases along the y direction. Thus, the result demonstrates that the planar stack adopted the U-type manifold configuration, instead of Z-type configuration, is promising to get similar pressure drop Δp throughout each piled cell unit. This pressure drop equals to the pressure difference between the inlet and outlet manifold sides. Similar pressure drop among the piled cell units means there are uniform air mass flow distribution among the piled cell layers.

The relevant normalized air flow rate distributions among the piled 20 cell units is shown in Fig. 5a. $\dot{m}_{r,i}$ is the normalized air mass-flow rate got by i -th cell layer. As described above, using normalized item to present the flow distributing quality can provide convenience in comparison among different stack designs. This air flow distributing quality is apparently better than that obtained basing on the 2in3out Z-type 20 cells stack as reported by Chen [8]. However, the air flow path with manifold configuration 2in3out, $r_{out}=r_{in}=4$ mm (i.e., case 1) and $\dot{m}_{air_in}=327$ SLPM still leads to a poor air flow distribution quality on stack level.

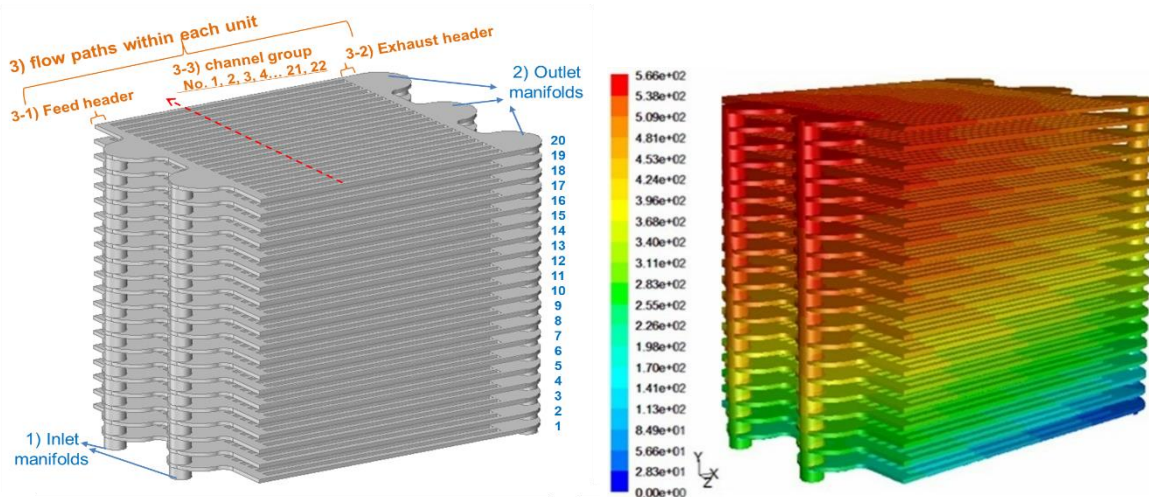


Figure 4. a) The 3D air flow field model within the 20-cell stack for case 1 labeled in table 3; b) the corresponding static pressure distribution within the air flow path.

There exist quite difference air flow rates between the first (near the manifold inlets) and last unit cells (20-th cell). The first unit cell gets the highest air mass flow rate, and 17-th unit cell gets the

lowest air flow rate as only 0.86 of the average mass flow rate. Therefore, the stack flow uniformity index for the case 1 stack is $\Gamma = 0.86$. As the cell that receives the least amount of gas flow rate may play the main role in affecting the overall SOFC stack performance, further parameters optimizing is essential to achieve a higher air flow distribution quality.

3.1. Optimization of stack level flow distribution

3.1.1. Air flow path

Fig. 5 compares the air flow rate $\dot{m}_{f,i}$ distributing profile among the 20 cells, while different manifold configurations and inlet/outlet manifold radii are adopted. The corresponding stack flow uniformity index Γ and the pressure drop throughout the whole stack are compared and discussed to achieve the proper SOFC performance.

For the 2in3out manifold configuration with $r_{out}=r_{in}$, Fig. 5a compares the $\dot{m}_{f,i}$ among the 20 unit cells for cases 1-5 in table 3 (i.e., the radii of the inlet/outlet manifolds $r_{in}=r_{out}=4, 5, 6, 7$ and 8 mm, listed). Generally, this 2in3out manifold configuration can be used in those modular short stacks with flow arrangement of type 1 (counter-flow with 2in3out for air flow path and 2in3out for fuel flow path) or type 3 (co-flow with 2in3out for air flow path and 3in2out for fuel flow path), as illustrated in table 2.

From Fig. 5a, we can get that the air flow distributing uniformity on stack level will increase with the increasing inlet/outlet manifold radii, while keep the air feed rate amount $\dot{m}_{air,in}=327$ SLPM. When the inlet/outlet manifold radii increase from 4 mm to 8 mm, stack flow uniformities index Γ are 0.86, 0.92, 0.94, 0.96 and 0.97, respectively, and the relevant pressure drop Δp are 274, 190, 153, 132 and 115 Pa, respectively.

Generally, one important consideration in SOFC stack structure designing is that “how to achieve the high flow uniformly distribution with a low total pressure drop between the inlet manifold entrance and outlet manifold exit”. Fortunately, the calculated result shows that increasing the inlet/outlet manifold radii may not only increase the stack uniformity Γ , but also can decrease the total stack pressure drop Δp . This conclusion is also consistent with the reported results [37]. Because of that the air flow rates obtained by cells are mainly determined by the pressure differences between the inlet and outlet manifolds. While the inlet/outlet manifolds radii increase, both the fluid velocities manifolds and pressure variation within the manifold decreases greatly.

Fig. 5b shows the normalized air flow rate distribution among the piled 20 unit cells in 3in2out manifold configuration with different inlet/outlet manifold radii. This manifold configuration model can be used in the modular short stack with flow arrangement of type 2 or type 4 as defined in table 2. As listed in table 3 case indexes 6 to 10 indicate the inlet/outlet manifold radii $r_{out}=r_{in}=4, 5, 6, 7$ and 8 mm, respectively. Obviously, comparing with the 2in3out manifold configuration cases, the 3in2out manifold configuration will lead to a smaller flow uniformity index and a higher total pressure drop on stack level. The relevant stack flow uniformity index Γ are collected in table 4 for further comparing in the following section.

Fig. 5c shows the air flow rate distribution conditions for the stack with 3in2out manifold configuration and a larger outlet manifold radius cases $r_{out}=1.2 r_{in}$. It clearly shows that using a larger outlet manifold radius can improve the air flow distributing uniformity among the cell units and reduce the pressure drop throughout the whole stack.

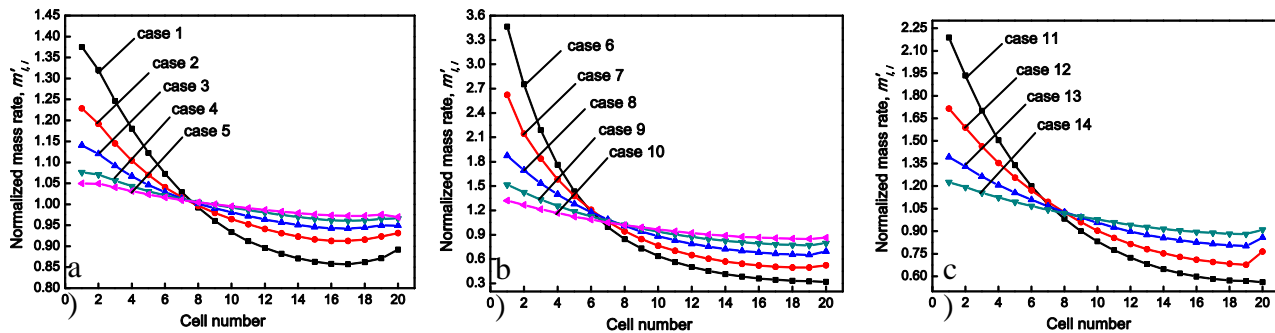


Figure 5. Air mass flow rate distributing profiles among the piled 20 cells for different flow manifold configurations, a) 2in3out with $r_{out}=r_{in}$, b) 3in2out with $r_{out}=r_{in}$; c) 3in2out with $r_{out}=1.2r_{in}$.

Table 4. Uniformity index for the stacks with different air flow manifold configurations and radii.

Manifold configuration	$r_{in}=4$	$r_{in}=5$	$r_{in}=6$	$r_{in}=7$	$r_{in}=8$	Support flow arrangement type
2in3out with $r_{out}=r_{in}$	0.86	0.92	0.94	0.96	0.97	Type 1 and 3
3in2out with $r_{out}=r_{in}$	0.32	0.50	0.65	0.77	0.85	Type 2 and 4
3in2out with $r_{out}=1.2r_{in}$	0.56	0.68	0.80	0.88		Type 2 and 4

*The unit for r_{in} is mm.

Table 4 summarizes the stack flow uniformity index Γ of three different manifold configurations: 2in3out with $r_{out}=r_{in}$, 3in2out with $r_{out}=r_{in}$, and 3in2out with $r_{out}=1.2r_{in}$. For the 20 cells modular short planar SOFC stack with the same inlet and outlet manifold radii, adopting the 2in3out air flow manifold configuration can lead to higher uniformity index Γ and lower pressure drop Δp than those adopting 3in2out manifold configuration. Additionally, increasing the inlet and outlet manifolds can improve the air flow distributing qualities on stack level. For the 2in3out air flow manifold configuration with $r_{out}=r_{in}$, while $r_{in} \geq 6$ mm, all the piled cell unit can obtained an air mass flow rate above 90% of the average value. For stack adopting the 3in2out air flow manifold configuration, choosing a large outlet manifold radius is considered to be an effective way to increase the stack flow uniformity.

3.1.2. Fuel flow path

Fig. 6 compares the fuel flow rate distributing profiles among piled 20 unit cells, while different manifold configurations and manifold radii are used. The case indexes and corresponding parameters are indicated in table 3. Fig. 6a shows the obtained normalized fuel mass flow rates

distributions among the piled cells for the 2in3out manifold configuration with $r_{out}=r_{in}$. This manifold configuration can be used in the flow arrangement patterns of Type 1 and type 4. Cases 21~25 are related to manifold radii from 4 to 8 mm, respectively. Fig. 6b shows the obtained normalized fuel mass flow rates distributions among the piled 20 cells for the 3in2out manifold configuration with $r_{out}=r_{in}$ (i.e., cases 26~30), and Fig. 6c for the 3in2out manifold configuration with a larger outlet radii $r_{out}=1.2r_{in}$ (i.e., cases 31~34). These results also well support the previous conclusion that enlarging the inlet/outlet manifold cross section areas would improve the distributing quality of air flow feeding rates among the piled 20-cells.

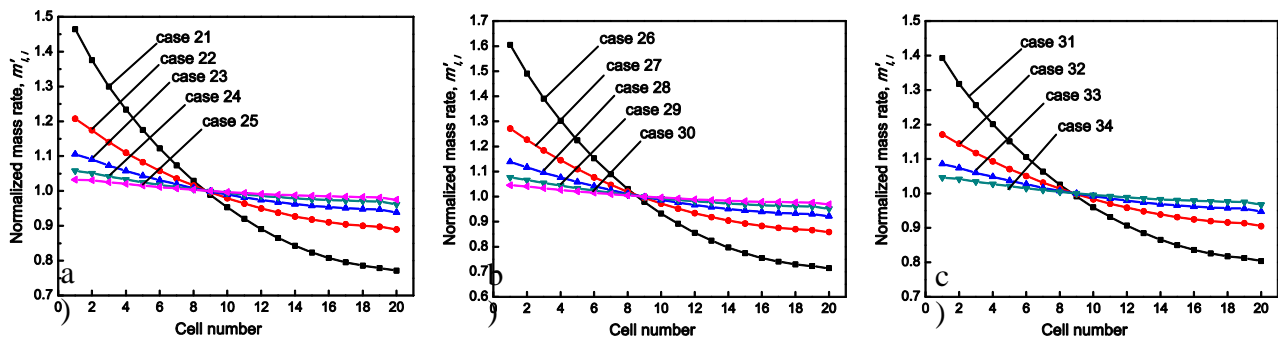


Figure 6. The distributing profiles of the obtained fuel mass flow rate among the piled 20 cells with different fuel flow manifold configurations, a) 2in3out with $r_{out}=r_{in}$; b) 3in2out with $r_{out}=r_{in}$; c) 3in2out with $r_{out}=1.2r_{in}$.

The calculated stack uniformity indexes are collected in table 5. For $r_{out}=r_{in}$ case, it shows that adopting the 2in3out manifold configuration would lead to a higher uniformity index and lower pressure drop than those stacks adopting the 3in2out configuration. This conclusion is well supported by the reported results in reference [8]. The inlet/outlet manifold radii around 6 mm are concluded to be a proper choice for the 20 cells SOFC stack to have a stack uniformity index of fuel flow distribution among the piled cell units above 0.9. Increasing the outlet manifold radius of the 3in2out configuration can improve the stack performance. For a larger outlet radius $r_{out}=1.2 r_{in}$ where $r_{in}=6$ mm, the stack uniformity index 0.95 can be achieved.

Table 5. Uniformity index for the stacks with different fuel flow manifold configurations and radii.

Manifold configuration		$r_{in}=4$	$r_{in}=5$	$r_{in}=6$	$r_{in}=7$	$r_{in}=8$	Support flow arrangement type
2in3out with $r_{out}=r_{in}$	Γ	0.77	0.89	0.94	0.96	0.98	Type 1 & 4
3in2out with $r_{out}=r_{in}$	Γ	0.71	0.86	0.92	0.95	0.97	Type 2 & 3
3in2out with $r_{out}=1.2r_{in}$	Γ	0.80	0.90	0.95	0.97		Type 2 & 3

* The unit r_{in} are Pa and mm, respectively.

Based on the calculated results summarized in tables 4 and 5, the following conclusions the 20 cells modular short planar SOFC stack with counter-flow or co-flow arrangement patterns can be reached:

i) The best counter-flow arrangement pattern for the 20 cells modular SOFC stack is Type 1, in which 2in3out manifold configuration is chosen for air flow path, and 2in3out manifold configuration for fuel flow path. The proper inlet and outlet manifold radii around 6 mm can well satisfy both the air/fuel flow distributing qualities and volumetric power density.

ii) The best co-flow arrangement pattern is Type 3, in which 2in3out manifold configuration is chosen for the air flow path, and 3in2out manifold configuration for the fuel flow path. Certainly, the 3in2out manifold configuration with $r_{out}=1.2r_{in}$ is considered to be a better choice, compared with the 3in2out manifold configuration with $r_{out}=r_{in}$. A inlet manifold radius around 6 mm is considered to be a proper value to well satisfy both the air/fuel flow distributing qualities and volumetric power density..

3.2. Optimizing the flow distribution quality among rib channels

Not only flow rate distributing quality among piled 20 cell layers, but also the flow rate distributing quality among the rib channels over each cell unit surface can greatly affect SOFC stack performance and its working lifetime. Distributing the flow rate evenly over each SOFC unit surface through rib channels is essential to achieve uniform electrochemical performance over the MEA and reducing the temperature gradient. As illustrated in Fig. 2, the manifold configuration, feed/exhaust header width, rib channel height, length and width, can affect the flow distributing quality among the rib channels. Although increasing the rib channel length or reducing the rib channel height can improve the mass flow rates distributing uniformity among the rib channels, it also will lead to a higher flow resistance. As reported by Lee [38], the serpentine flow field pattern shown better flow distributing quality than that in convenient parallel flow field pattern. Tran had reviewed many different flow field designs over the polymer electrolyte membrane fuel cell surfaces and concluded that multi-pass serpentine flow field could support more uniform gas distributions on cell unit level [39]. However, adopting the serpentine flow field will increase the flowing resistance within rib channels; and this means additional pump is required. In this section, we would optimize the feed/exhaust header width to achieve the high quality mass flow rate distribution among the rib channels. Generally, although adjusting the feed/exhaust header width may not greatly affect the total pressure drop within the stack, it would greatly affect the flow distributing quality among the rib channels

3.2.1 Header width for air manifold configuration 2in3out

Fig. 7 illustrates the effects of various feed/exhaust header widths on the normalized air mass flow rates distributions for 2in3out manifold configuration with $r_{out}=r_{in}=6$ mm. In Fig. 7a the calculated result seems that the air flow distributions among the piled 20 unit layers are insensitive to the change of the feed/exhaust header width. Fig. 7b shows the dependence of air flow distributions among the rib channels on the feed/exhaust header widths. Obviously, the air flow distribution quality on cell unit level will be greatly affected by the feed/exhaust header width. The rib channels at both

corners (i.e., the first and 22-th channels) will get the minimal air mass flow rates. Increasing the feed/exhaust header width can greatly improve the air mass flow distributing quality among the rib channels. When the feed/exhaust header widths increase from 2.5 to 15 mm, the normalized air mass flow rates obtained by the first and 22-th channels will increase from 0.83 to 0.96 of the average mass flow rates. Since all the rib channels over each cell unit surface are connected in parallel, standard deviation factor σ_c is considered to be a more effective factor to indicate the air flow distribution quality among the rib channels.

For the feed/exhaust header widths of 2.5, 5, 10 and 15 mm, the standard deviation factors σ_c for the air mass flow rates obtained by the rib channels are 0.107, 0.047, 0.024 and 0.017, respectively. The standard deviation factor decreases with the increasing feed/exhaust header width; and a feed/exhaust header width larger than 10 mm can be considered as a proper width for the 20 cells modular short SOFC stack with the 2in3out air manifold configuration to achieve reasonable good air flow distribution quality among the rib channels.

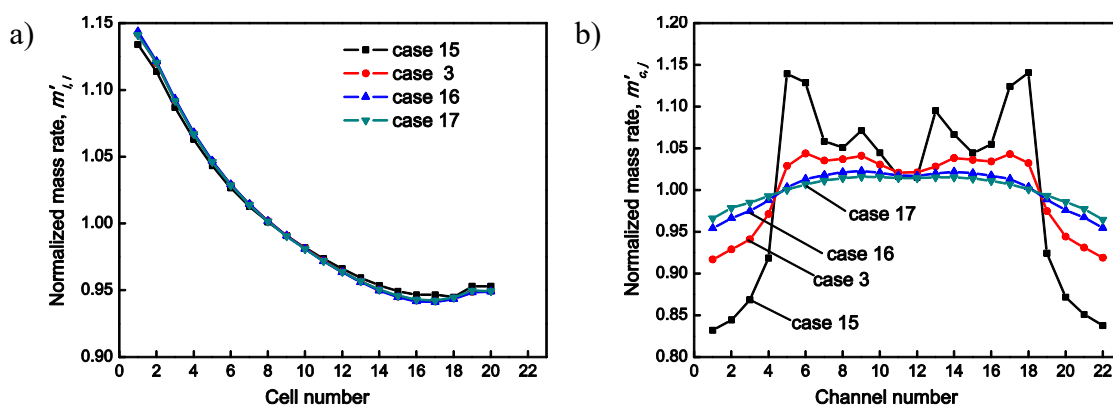


Figure 7. Effects of various feed/exhaust header widths on the air flow distribution qualities on both stack and cell unit levels for the case of 2in3out air manifold configuration with $r_{out}=r_{in}=6$ mm, a) normalized air mass flow rates among the 20 unit cells; b) normalized air mass flow rates among the rib channels.

3.2.2 Header width for fuel manifold configurations 2in3out and 3in2out

Similar, Fig. 8 shows the effects of various feed/exhaust header widths on the normalized fuel mass flow rates distributions for the 2in3out manifold configuration with $r_{out}=r_{in}=6$ mm. Fig. 8a shows that the fuel flow rates among the piled 20 cells is not sensitive to the variation of feed/exhaust header width. Fig. 8b shows the effects of the feed/exhaust header width on normalized fuel mass flow rates $m'_{c,j}$ among the rib channels. Obviously, the feed/exhaust headers will greatly affect the distribution quality of the fuel mass flow rates obtained by the rib channels. While the feed/exhaust header width increase from 2.5 mm to 15 mm, the fuel mass flow rates obtained by the first and 22-th rib channels increase from 0.78 to 0.96 of the mean fuel mass flow rates. The standard deviation factors σ_c are 0.113, 0.055, 0.027 and 0.019, while the feed/exhaust header widths are set to 2.5, 5, 10 and 15 mm,

respectively. Then, a feed/exhaust header width larger than 10 mm is also considered to be a proper value for the 20 cells modular short planar SOFC stack with 2in3out fuel manifold configuration to achieve a standard deviation factors less than 0.027.

Fig. 9 shows the effects of various feed/exhaust header widths on the fuel flow distribution qualities on both stack and cell unit levels for the case of 3in2out $r_{out}=1.2r_{in}$ and $r_{in}=6$ mm, The relevant standard deviation factors σ_c are 0.098, 0.047, 0.024 and 0.017, while the feed/exhaust header widths equal to 2.5, 5, 10 and 15 mm, respectively. Obviously, the rib channel configurations and the feed/exhaust header widths are two important geometric factors to affect the air flow distributing quality among the rib channels (or over each cell unit surface).

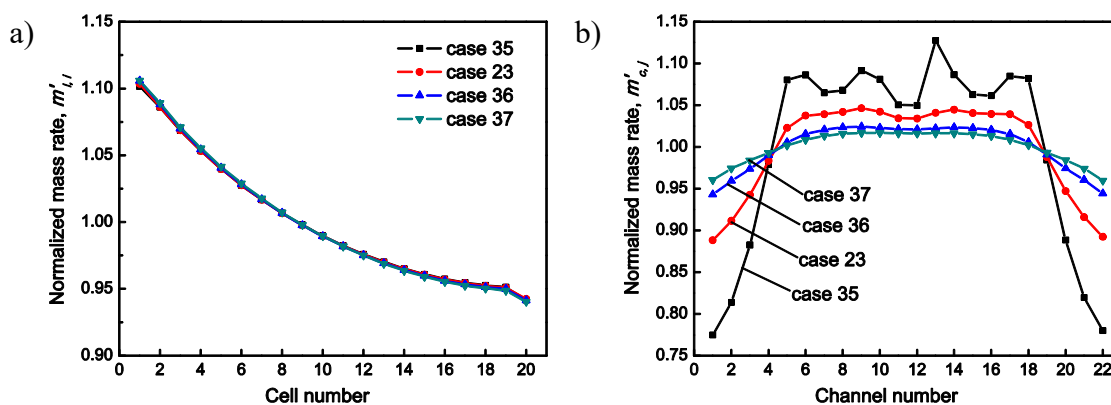


Figure 8. Effects of various feed/exhaust header widths on the fuel flow distribution qualities on both stack and cell unit levels for the case of 2in3out air manifold configuration with $r_{out}=r_{in}=6$ mm, a) normalized fuel mass flow rates among 20 unit cells; b) normalized fuel mass flow rates among rib channels.

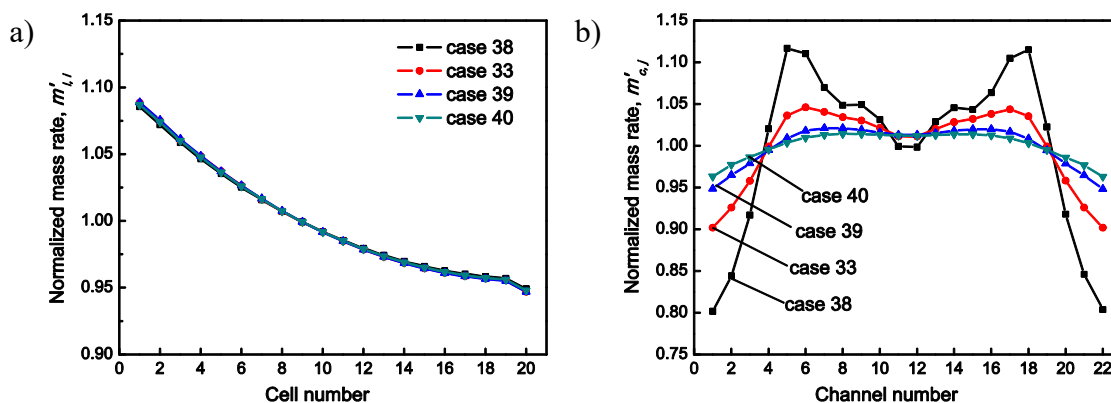


Figure 9. Effects of various feed/exhaust header widths on the fuel flow distribution qualities on both stack and cell unit levels for the case of 3in2out $r_{out}=1.2r_{in}$ and $r_{in}=6$ mm, a) mass flow rates among 20 unit cells; b) mass flow rates among rib channels.

As reported by Duy, although adjusting the cross-sectional area of gas flow channel could affect the flow distributing quality over cell unit surface, it would also greatly influence the pressure drop within the stack [40]. However, from the optimized result in this section we can get that although

adjusting the feed/exhaust header widths will affect the air flow districting quality among the rib channels, both the air flow distributing quality on stack level and total pressure drop throughout the whole stack will be not sensitive to this geometric adjustment.

Table 6 conclusively summarizes the standard deviation factors of $\dot{m}_{c,j}$ for various manifold configurations with different feed/exhaust header widths; and the following conclusions can be achieved.

i) Type 3 will be the best co-flow arrangement pattern chooses for this 20 cells modular stack, the proper optimized air flow path is case 16, in which the inlet/outlet radii are 6 mm, and the feed/exhaust header widths are 10 mm. The best fuel flow path is case 39 with the feed/exhaust header widths of 10 mm, and the stack uniformity index is 0.94 and standard deviation factor is 0.024.

ii) Type 1 will be the best counter-flow arrangement chooses for this 20-cells modular stack. The best air flow path is case 16, in which the inlet/outlet radii are 6 mm and the feed/exhaust header widths are 10 mm. The stack uniformity index is 0.94, standard deviation factor is 0.024, and the pressure drop is 153 Pa. The best fuel flow path is case 36, in which the inlet/outlet radii are 6 mm and the feed/exhaust header widths are 10 mm. The stack uniformity index is 0.94 and standard deviation factor is 0.027.

Table 6 Standard deviation factor for the distribution of the mass flow rates obtained by the rib channels

Air flow manifold: 2in3out with $r_{out}=r_{in}=6$ mm				
Header width (mm)	2.5	5	10	15
σ_c	0.107	0.047	0.024	0.017
Fuel flow manifold: 2in3out with $r_{out}=r_{in}=6$ mm				
Header width (mm)	2.5	5	10	15
σ_c	0.113	0.055	0.027	0.019
Fuel flow manifold: 3in2out with $r_{out}=1.2r_{in}$, $r_{in}=6$ mm				
Header width (mm)	2.5	5	10	15
σ_c	0.098	0.047	0.024	0.017

4. CONCLUSIONS

The 3D large scale computational fluid dynamic models for the air and fuel flow paths within the 0.5~1.5 kW modular short planar SOFC stack with 20 unit cells were developed. They were used to compare and optimize the air and fuel paths of these SOFC stacks at both stack and unit cell levels. The stack uniformity index which was the least gas flow rate obtained by the 20 unit cells, pressure drop, and the standard deviation factor of gas mass flow rates obtained by the rib channels were used to characterize the qualities of flow distributions within the air and fuel flow paths. Geometric parameters, such as the manifold configurations, inlet/outlet manifold radii and feed/exhaust header

widths are investigated; and the optimized geometric parameters for these modular short planar SOFC stack with both counter- or co-flow arrangement patterns were concluded.

ACKNOWLEDGEMENTS

We gratefully acknowledge the financial support of the National Natural Science Foundation of China (21106058 and 51776092), the Natural Science Foundation of Jiangsu Province General Program (BK20151325), the Jiangsu Province “333” High Level Talent Project.

CONFLICT OF INTEREST

The authors declare that they have no conflict of interest.

Reference

1. T.C. Patil, S.M. Mahajani, S.P. Dutttagupta. *Int. J. Electrochem. Sci.*, 9 (2014) 8458.
2. D. Chen, H. Wang, S. Zhang, M.O. Tade, Z. Shao, H. Chen. *AIChE J.*, 61 (2015) 3786.
3. S. Sugita, H. Arai, Y. Yoshida, H. Orui, M. Arakawa. *ECS Trans.*, 5 (2007) 491.
4. L. An, T. Zhao, X. Yan, X. Zhou, P. Tan. *Sci. Bull.*, 60 (2015) 55.
5. K. Zheng, M. Ni. *Sci. Bull.*, 61 (2016) 78.
6. D. Chen, Q. Zhang, L. Lu, V. Periasamy, M.O. Tade, Z. Shao. *J. Power Sources*, 303 (2016) 305.
7. Z. Qu, M. Shi, H. Wu, Y. Liu, J. Jiang, C. Yan. *J. Power Sources*, 410-411 (2019) 179.
8. D. Chen, Y. Xu, M.O. Tade, Z. Shao. *Acs. Energy Lett.*, 2 (2017) 319.
9. W. Kong, W. Zhang, S. Zhang, Q. Zhang, S. Su. *Int. J. Hydrogen Energy*, 41 (2016) 16173.
10. D. Chen, L. Lu, J. Li, Z. Yu, W. Kong, H. Zhu. *J. Power Sources*, 196 (2011) 3178.
11. L. Lu, W. Zeng, S. Hu, D. Chen, J. Lei, N. Ren. *J. Alloys Compd.*, 731 (2018) 753.
12. F.X. Miao. *Int. J. Electrochem. Sci.*, 8 (2013) 11814.
13. Z. Yu, S. Liu, F. Zheng, Y. Ding. *Int. J. Electrochem. Sci.*, 11 (2016) 10210.
14. D. Chen, B. Hu, K. Ding, C. Yan, L. Lu. *Energies*, 11 (2018) 1875.
15. L. Blum, S.M. Groß, J. Malzbender, U. Pabst, M. Peksen, R. Peters. *J. Power Sources*, 196 (2011) 7175.
16. A.I. Marquez, T.R. Ohrn, J.P. Trembly, D.C. Ingram, D.J. Bayless. *J. Power Sources*. 164 (2007) 659.
17. N.M. Sammes, Y. Du, R. Bove. *J. Power Sources*, 145 (2005) 428.
18. W. Kong, X. Gao, S. Liu, S. Su, D. Chen. *Energies*, 7(2014) 295.
19. R.J. Kee, P. Korada, K. Walters, M. Pavol. *J. Power Sources*, 109 (2002) 148.
20. M. Peksen. *Int. J. Hydrogen Energy*, 36 (2011) 11914.
21. D. Chen, Y. Xu, B. Hu, C. Yan, L. Lu. *Energ. Convers. Manage.*, 171 (2018) 807.
22. S. Su, H. He, D. Chen, W. Zhu, Y. Wu, W. Kong. *Int. J. Hydrogen Energy*, 40 (2015) 577.
23. C.M. Huang, S.S. Shy, C.H. Leeb. *J. Power Sources*, 183 (2008) 205.
24. H.Y. Jung, S.H. Choi, H. Kim, J.W. Son, J. Kim, H.W. Lee. *J. Power Sources*, 159 (2006) 478.
25. H. Chen, F. Wang, W. Wang, D. Chen, S.-D. Li, Z. Shao. *Appl. Energ.*, 179 (2016) 765.
26. K. Liu, B. Liu, R. Villavicencio, Z. Wang, C. Guedes Soares. *Ships Offshore Struc.*, 13 (2018) 217.
27. L. Lu, X. Xu, W. Liang, H. Lu. *J. Phys Condens. Mat.*, 19 (2007) 406221.
28. R.J. Boersma, N.M. Sammes. *J. Power Sources*, 63 (1996) 215.
29. J.H. Myung, H.J. Ko, J.-J. Lee, S.H. Hyun. *Int. J. Electrochem. Sci.*, 6 (2011) 1617.
30. G. Hu, X. Wu, Y. Suo, Y. Xia, Y. Xu, Z. Zhang. *Int. J. Electrochem. Sci.*, 13 (2018) 2080.
31. K.P. Recknagle, R.E. Williford, L.A. Chick, D.R. Rector, M.A. Khaleel. *J. Power Sources*, 113 (2003) 109.

32. D. Chen, K. Ding, Z. Chen, T. Wei, K. Liu. *Energ. Convers. Manage.*, 178 (2018) 190.
33. S. Su, S. Zhang, C. Yan, Z. Yang, F. Zheng, L. Zhang. *Int. J. Electrochem. Sci.*, 12 (2017) 230.
34. D. Chen, Q. Zeng, S. Su, W. Bi, Z. Ren. *Appl. Energ.*, 112 (2013) 1100.
35. H.S. Song, S. Lee, D. Lee, H. Kim, S.H. Hyun, J. Kim. *J. Power Sources*, 195 (2010) 2628.
36. M. Yokoo, Y. Tabata, Y. Yoshida, K. Hayashi, Y. Nozaki, K. Nozawa. *J. Power Sources*, 190 (2009) 252.
37. S.C. Su, S.D. Zhang, C. Yan, Z.M. Yang, F. Zheng, L. Zhang. *Int. J. Electrochem. Sci.*, 12 (2017) 230.
38. B. Lee, K. Park, H.M. Kim. *Int. J. Electrochem. Sci.*, 8 (2013) 219.
39. T.T. Diep, S. Huang, V.D. Ha, D.V. Nguyen. *Int. J. Electrochem. Sci.*, 13 (2018) 10480.
40. D.V. Nguyen, K. Kim, J. Lee, J. Ahn, S. Park, T. Kim. *Int. J. Electrochem. Sci.*, 10 (2015) 5842.

© 2019 The Authors. Published by ESG (www.electrochemsci.org). This article is an open access article distributed under the terms and conditions of the Creative Commons Attribution license (<http://creativecommons.org/licenses/by/4.0/>).